ISSN 1063-7826, Semiconductors, 2017, Vol. 51, No. 5, pp. 576–581. © Pleiades Publishing, Ltd., 2017.
Original Russian Text © A.A. Zarubanov, V.F. Plyusnin, K.S. Zhuravlev, 2017, published in Fizika i Tekhnika Poluprovodnikov, 2017, Vol. 51, No. 5, pp. 605–610.

SPECTROSCOPY, INTERACTION WITH RADIATION

Electronic Excitation Transfer from an Organic Matrix to CdS Nanocrystals Produced by the Langmuir–Blodgett Method

A. A. Zarubanov[a]*, V. F. Plyusnin[b, c], and K. S. Zhuravlev[a, c]

[a] *Institute of Semiconductor Physics, Siberian Branch, Russian Academy of Sciences, Novosibirsk, 630090 Russia*
[b] *Voevodsky Institute of Chemical Kinetics and Combustion, Siberian Branch, Russian Academy of Sciences, Novosibirsk, 630090 Russia*
[c] *Novosibirsk State University, Novosibirsk, 630090 Russia*
**e-mail: alexsundr@mail.ru*

Submitted November 8, 2016; accepted for publication November 14, 2016

Abstract—The absorption, photoluminescence, and photoluminescence excitation spectra of CdS nanocrystals formed by the Langmuir–Blodgett method are explored. Features of the absorption and photoluminescence excitation spectra defined by optical transitions in the matrix and nanocrystals are identified. The efficiency of electronic excitation transfer from an organic matrix to nanocrystals is studied. It is shown that charge carriers efficiently transfer from the matrix to electron and hole size-quantization levels in nanocrystals and to acceptor defect levels in the band gap of nanocrystals. A large Stokes shift defined by fine exciton structure (bright and dark excitons) is observed. The shift is in the range 140–220 meV for nanocrystals 2.4 and 2.0 nm in radius.

DOI: 10.1134/S1063782617050268

1. INTRODUCTION

In the last few years, nanocrystals (NCs) based on II–VI semiconductors have been extensively studied because of their high potential for applications in various nanoelectronic devices. NCs are produced mainly by molecular-beam epitaxy (MBE) and nanolithography. The comparatively simple and less expensive methods of production of NCs are the methods of colloidal chemistry and the Langmuir–Blodgett (LB) method [1]. The LB method implies the presence of a solid organic matrix that can be removed if necessary [2]. Organic materials in combination with semiconductor NCs offer promise for the production of solar cells [3–6]. In such structures, a key role is played by the processes of electronic excitation transfer from the organic matrix to NCs [6–11].

Electronic excitation transfer from the matrix to NCs has been extensively studied for NCs embedded in a semiconductor matrix [12–15] and for NCs in conducting poly[2-methoxy,5-(2-ethylhexyloxy)-1.4-phenylenevinylene] (MEH-PPV) organic compounds [5, 9, 16]. In the last-mentioned case, electron or hole transfer as well as exciton transfer were observed. The electronic excitation transfer from an organic LB matrix to NCs is poorly understood.

In this study, to explore the processes and efficiency of electronic excitation transfer from an organic matrix to NCs, we analyze the absorption spectra and the photoluminescence excitation (PLE) spectra of NCs before and after annealing of the matrix.

2. EXPERIMENTAL

The CdS NC samples to be studied were produced by the LB technique. For substrates, we used (1000)-oriented sapphire, onto which 80 cadmium-behenate single layers were deposited. The single-layer thickness of the LB film is about 2.7 nm. The cadmium-behenate films were sulfurized with gaseous hydrogen sulfide (H_2S) at a temperature of 22°C and H_2S pressure of 100 Torr for 2 h. Upon the interaction of cadmium behenate with hydrogen sulfide, cadmium-sulfide NCs distributed in an insulating begenic-acid matrix (sample Matrix) were formed. The LB matrix was removed by the thermal desorption of behenic acid in an ammonia atmosphere at a temperature of 150 and 200°C (samples NC150 and NC200, respectively) for ~2 h, and the NCs remained on the substrate surface.

According to the high-resolution transmission electron microscopy (TEM) data shown in Figs. 1a and 1b, the NC radius in the matrix varies from 1.0 to 1.9 nm, and the average NC radius is ~1.7 nm. The density of NCs is ~10^{11} cm^{-2}. The NCs occupy ~1% of the sample area. After annealing at 200°C, the NC radius is increased and corresponds to ~2.5 nm (Figs. 2a, 2b).

The photoluminescence (PL) and PLE spectra were recorded at room temperature, using an FLS920 spectrofluorimeter with a 450-W xenon lamp as the excitation source. The absorption spectra were studied

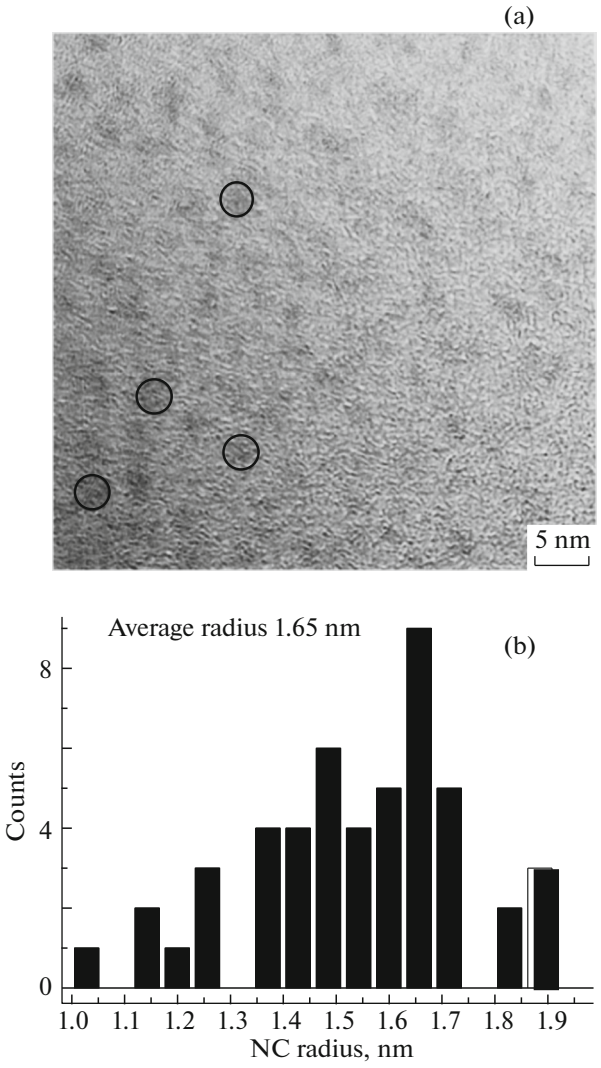

Fig. 1. (a) TEM image of the sample containing CdS NCs in the matrix with a thickness of 10 single layers. (b) Histogram of the distribution of NCs in radius.

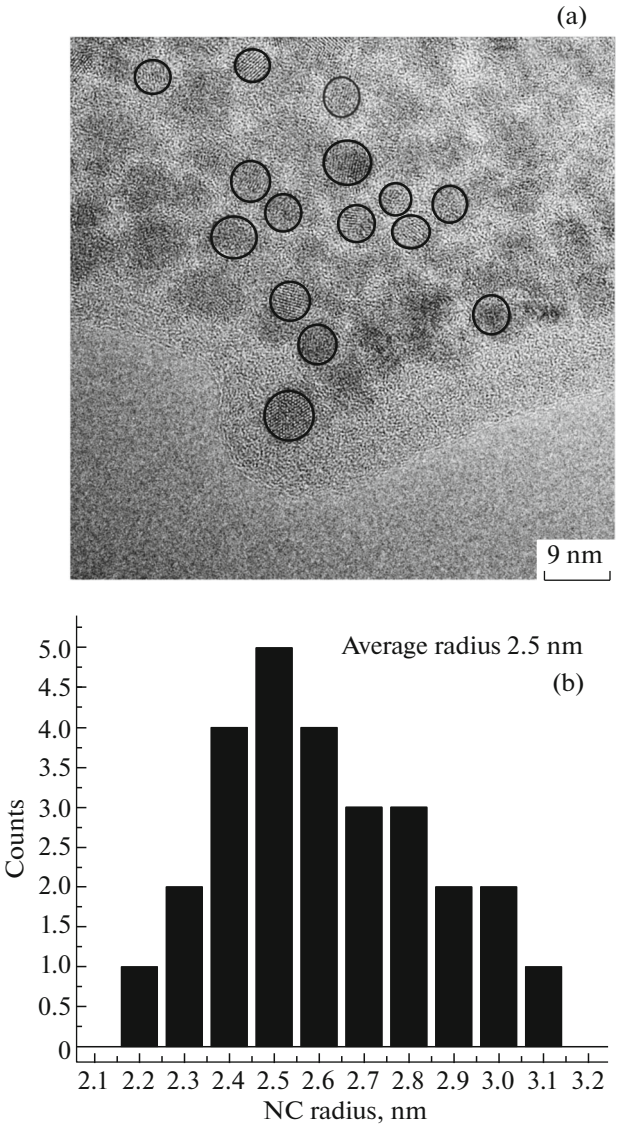

Fig. 2. (a) TEM image of the sample containing CdS NCs in the matrix with a thickness of 10 single layers after annealing at 200°C. (b) Histograms of the distribution of NCs in radius.

using an Acton SP2500 (Princeton Instruments) spectrometer, with recording of the signal with a CCD camera cooled by liquid nitrogen. For the light source, we used an Ocean Optics D1000 deuterium lamp.

3. RESULTS

Figure 3 shows the absorption spectra of samples with CdS NCs in the matrix and of CdS NCs samples after thermal desorption of the matrix at temperatures of 150 and 200°C. For all three samples, the optical absorbance increases, as the wavelength of absorbed light is decreased. At the same time, in the visible region of the spectra of samples Matrix, NC150, and NC200, there are absorption peaks at wavelengths of 365, 405 and 430 nm, respectively. The absorption spectrum of sample Matrix exhibits a low-intensity peak around 270 nm. In the ultraviolet (UV) region, the absorption spectra of samples Matrix, NC150, and NC200 exhibit peaks at 215, 220, and 225 nm, respectively.

Figure 4 shows the PL spectra of samples Matrix, NC150, and NC200. In the PL spectra of all of the samples, a broad band lying in the wavelength range 450–800 nm is dominant, and for samples Matrix, NC150, and NC200, there is a PL band with a lower intensity, with a peak at 435, 455, and ~400 nm, respectively.

Figure 5a shows the PLE spectra recorded at an energy corresponding to the maximum of the short-wavelength PL peak. In the PLE spectra of all three samples, we observe peaks with a maximum at ~270 nm. In the spectra of samples NC150 and

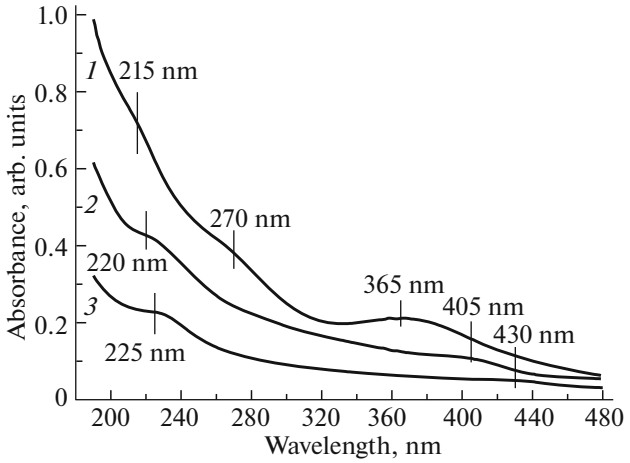

Fig. 3. Absorption spectra of samples with CdS NCs on sapphire substrates: (*1*) CdS NCs in the matrix and (*2*, *3*) CdS NCs after thermal desorption of the matrix at the temperatures (*2*) 150 and (*3*) 200°C.

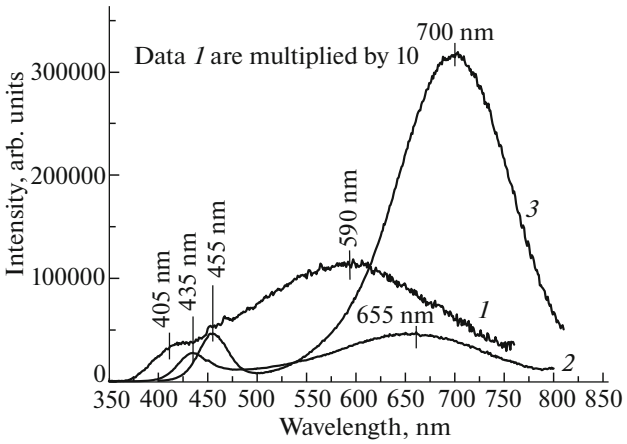

Fig. 4. PL spectra of samples with CdS NCs on sapphire substrates: samples (*1*) Matrix, (*2*) NC150, and (*3*) NC200.

NC200, we can see an additional peak with a maximum at ~365 nm. The most pronounced differences are observed in the short-wavelength region of the PLE spectra. In the spectra of samples Matrix and NC150, a peak at ~215 nm is dominant; however, its intensity in sample NC150 is much lower. In the spectrum of sample NC200, the intensity of the short-wavelength peak is even lower; the peak is shifted to the red region of the spectrum and exhibits a maximum at ~240 nm.

The PLE spectra, for which the energy of recording of the emission signal corresponds to the maximum of the long-wavelength PL peak, are shown in Fig. 5b. The PL intensity decreases, as the energy of the excitation light is decreased. In contrast to the PLE spectra recorded for the short-wavelength PL peak, in the spectra of samples Matrix, NC150, and NC200, the positions of the PL maxima in the UV region are shifted to longer wavelengths and observed at 220, 230, and 240 nm, respectively. The intensity of these PL peaks decreases, as the annealing temperature of the sample is increased. As in the PLE spectra recorded for the short-wavelength peak, the 270 and 365 nm maxima are observed in the spectra of all of the samples. The PLE spectra of samples NC150 and NC200 exhibit peaks in the blue spectral region, at ~405 and ~435 nm, respectively.

4. DISCUSSION

The short-wavelength PL peak (Fig. 4) is defined by optical transitions between size-quantization levels in NCs [17]. The shift of this PL peak to longer wavelengths is due to an increase in the NC size with increasing annealing temperature [17]. The position of the short-wavelength PL peak is related to the NC dimensions by Brus's formula which takes into account the quantum-confinement effect and Coulomb interaction between an electron and a hole [18]:

$$E = E_{g0} + \frac{\hbar^2\pi^2 n^2}{2m^* R^2} - \frac{1.8e^2}{4\pi\varepsilon\varepsilon_0 R}. \quad (1)$$

Here, E is the energy separation between the electron and hole size-quantization levels, $E_{g0} = 2.48$ eV is the band gap of bulk CdS at the temperature $T = 300$ K, $\hbar$ is Planck's constant, n is a positive integer, $m^* = m_e m_h/(m_e + m_h) = 0.154m_0$ is the reduced mass of an electron ($m_e = 0.19m_0$) and a hole ($m_h = 0.8m_0$), e is the elementary charge, ε is the permittivity of CdS ($\varepsilon = 5.7$ [18]), ε_0 is the permittivity of free space, and R is the NC radius. Calculation by the above formula shows that, in samples Matrix, NC150, and NC200, the NC radius is 1.7, 2.0, and 2.4 nm, respectively. According to the TEM data, the average NC radius is 1.7 nm for sample Matrix and 2.5 nm for sample NC200, which supports the above estimates.

The broad PL peak in the long-wavelength region of the spectrum is defined by recombination through energy levels arranged in the band gap of NCs. These levels can be attributed to structural defects within NCs as well as to states at the NC–matrix interface. Figure 4 shows the positions of both PL peaks for NCs different in size. It can be seen that, with increasing NC radius, both peaks shift to lower energies in a similar manner. The energy separation between the peaks is ~0.95 eV and remains unchanged under variations in the NC size. It is known that the position of a defect level in NCs only slightly depends on the NC size [19]. Therefore, the shift of the long-wavelength peak can be attributed to the shift of the size-quantization level, if the transition occurs between the size-quantization level and the defect level.

Figure 6 shows the electron and hole energies in NCs, as calculated in accordance with the above for-

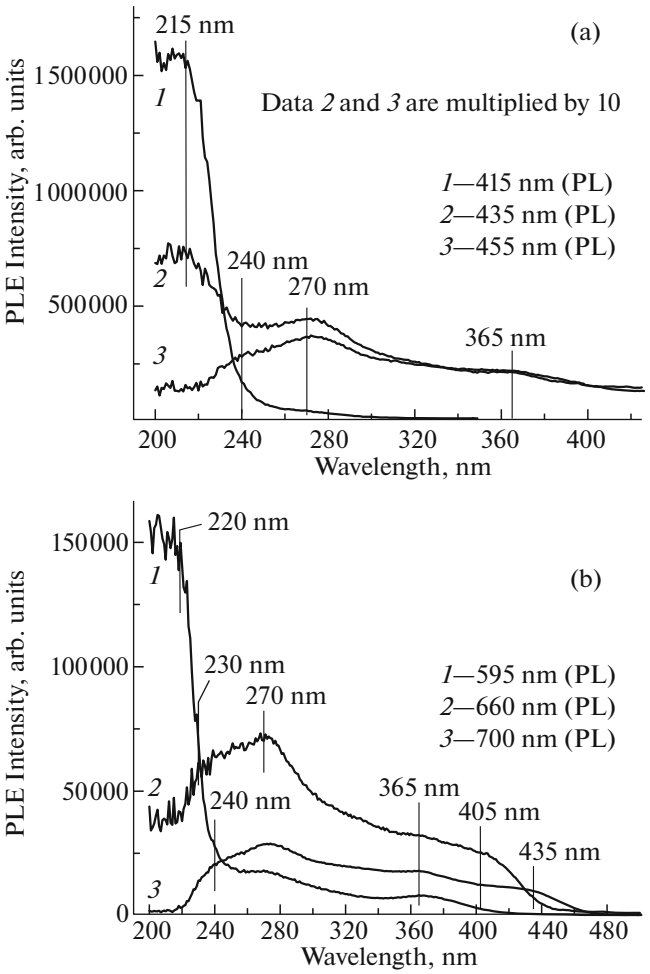

Fig. 5. PLE spectra of samples with CdS NCs for the (a) short- and (b) long-wavelength PL peaks: samples (*1*) Matrix, (*2*) NC150, and (*3*) NC200. The wavelengths of recording the PL signal are denoted by the abbreviation PL.

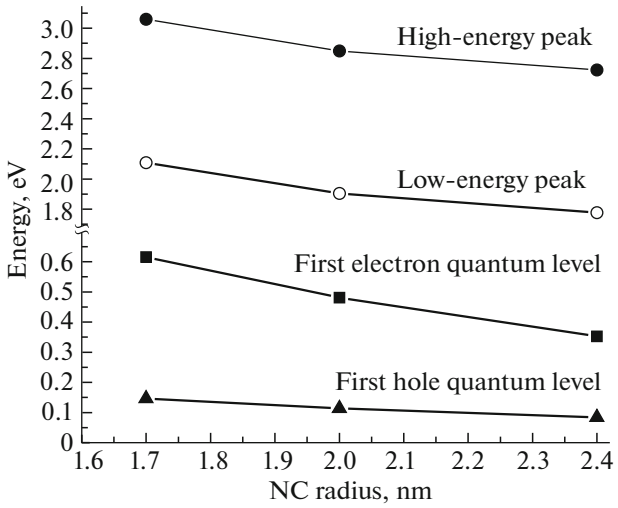

Fig. 6. Dependence of the positions of PL peaks and electron and hole size-quantization levels on the NC size.

mula. To calculate the size-quantization energy by this formula, we used the electron or hole effective masses instead of the reduced mass of an electron and a hole. From Fig. 6, it can be seen that, under variations in the NC size, the electron level shifts more markedly (ΔE_e) than the hole level (ΔE_h) because of the large difference between the electron and hole effective masses ($m_e < m_h$). Moreover, it can be seen that, under variations in NC size, the electron level and PL peaks shift symbatically. Consequently, the shift of the PL peaks is defined by the change in the energy of electrons.

Electron transitions between size-quantization levels in NCs manifest themselves in the visible region (405–450 nm) of the absorption spectra and the excitation spectra of the long-wavelength PL peak in samples NC150 and NC200. The fact that the peak defined by transitions in NCs is lacking in the visible region of the absorption and PLE spectra in sample Matrix can be interpreted as a result of absorption mainly in the matrix. This is obviously because of the fact that, at comparable thicknesses, the matrix accounts for about 99% of the sample area, whereas the NCs account for only about 1%. Upon annealing, the matrix is thinned and/or decreased in area, and absorption in NCs becomes comparable to absorption in the matrix. It seems likely that, upon annealing, absorption in the matrix is reduced in a larger part because of the decrease in its area.

From comparison of the positions of peaks in the PL and PLE spectra, we can estimate the Stokes shift. It is found that the Stokes shift is 140 and 220 meV, correspondingly, for samples NC150 and NC200, in which the average NC radius is 2.4 and 2.0 nm, respectively. Such a large Stokes shift is caused by the fine exciton structure. In this case, the absorption of light is defined by transitions to the level of a bright exciton, and emission by the annihilation of a dark exciton [20]. Previously, for CdS NCs produced by methods of colloidal chemistry, the Stokes shift observed for NCs with the radii 2.0 and 1.3 nm at a temperature of 10 K was 20 and 70 meV, respectively [20]. These values are several times smaller than the values obtained in this study. Such a difference can be due to the effect of the NC surroundings [21].

The bands observed in the UV region of the absorption and PLE spectra (at 270 nm and in the wavelength range 215–240 nm) are most likely due to absorption in the matrix or its remnants. Such an interpretation is supported by the fact that no such bands were observed in the absorption spectra of sapphire, but were evident in the PLE spectra of NCs on a silicon substrate. In addition, the calculation of the energies of size-quantization levels by the above formula (1) shows that, in NCs, the transitions corresponding to the energies of the maxima of these bands are lacking. The energies of transitions between the

second electron and hole size-quantization levels in samples NC200, NC150, and Matrix are, correspondingly, 4.0, 4.7, and 5.6 eV (305, 265, and 225 nm) which are lower than the energies of experimentally observed transitions. The decrease in the intensity of the short-wavelength band in the PLE spectra by an order of magnitude with increasing annealing temperature is attributed to thermal desorption of the matrix, and the shift of this band from 215 to 240 nm can be attributed to some change in the composition of the matrix. The PLE spectra make possible rather accurate estimation of the band gap of the matrix of the initial LB film; the estimated band gap is 5.8 eV. After annealing at 200°C, the band gap of the remnants of the matrix is 5.1 eV, which is in agreement with the value obtained in [22]. We think that the ~270-nm band in the PLE spectra is associated with states at the NC–matrix interface, since annealing of the matrix does not influence the intensity of this band and, according to calculations, the corresponding transitions are lacking in the spectrum of NCs. The 366-nm band is apparently associated with levels in the band gap of the matrix. This is suggested by the high intensity of this band in the spectrum of the unannealed sample and by the decrease in absorption with respect to absorption in the blue spectral region after annealing. A similar situation is observed in the PLE spectrum of the defect-related PL band (Fig. 5b). However, the maxima of the UV bands in the PLE spectra of samples Matrix and NC150 are shifted to the red spectral region and arranged at ~220 and ~230 nm, respectively. The physical cause of such changes is now unclear.

From the PLE spectra, it can be seen that electron–hole (e–h) pairs generated in the matrix are trapped and recombine in NCs. The NCs trap e–h pairs from the matrix (215-nm band) and from states at the NC–matrix interface (~270- and ~365-nm bands). This is confirmed by the observation of high intensities of PLE bands defined by absorption in the matrix. By comparing the absorption and PLE spectra, we can judge the efficiency of excitation transfer from band states (215-nm band) and defect states in the matrix (270- and 365-nm bands). Figure 7 shows the wavelength dependence of the efficiency of excitation transfer (the dependence is determined as the ratio of the PLE spectrum to the absorption spectrum). In such a comparison of the efficiencies of transfer from different states of the matrix, the losses to nonradiative recombination in NCs should not be taken into account. From Fig. 7, it can be seen that, for sample Matrix, the efficiency of excitation transfer from defect states of the matrix to NCs is lower than that from band states of the matrix. The relative efficiency of excitation transfer from defect states of the matrix to NCs is about 5%. As the annealing temperature is elevated, the efficiency of excitation transfer from the matrix decreases with respect to the efficiency of transfer from defect states of the matrix. This

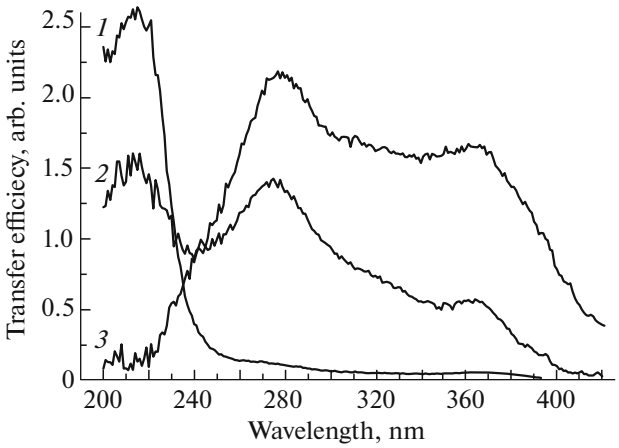

Fig. 7. Wavelength dependence of the efficiency of electronic excitation transfer to NCs for samples (*1*) Matrix, (*2*) NC150, and (*3*) NC200.

is probably due to some changes in the structure of the matrix. The heat treatment of thin organic semiconductor layers can modify the interfaces between layers and their internal structure, which affects, among other properties, the luminescence and induces its quenching [23].

When entering NCs, charge carriers generated in the matrix can recombine also through an acceptor level and, thus, give a defect-related PL signal (Fig. 5b). In this case, a hole can be trapped directly at the acceptor level or be incident on this level through the hole size-quantization level in a NC. The intensity of the UV band in the PLE spectrum of sample Matrix is an order of magnitude higher than the intensity of a similar band in the PLE spectrum of the defect band. This means that the major fraction of charge carriers generated in the matrix is incident on the size-quantization levels of NCs and only a minor fraction is trapped by the acceptor level. At the same time, the dominant channel of radiative recombination is that through the acceptor level. With consideration for the aforesaid, we can conclude that charge carriers are incident from the matrix on the size-quantization level and then are incident on the acceptor level and recombine.

The intensities of the ~270- and ~365-nm bands in the PLE spectra of NCs and the intensity of the defect band are nearly equal for all of the samples. Moreover, in the PLE spectra of the defect band of samples NC150 and NC200, the bands defined by states at the matrix–NC interface (270 and 365 nm) are higher in intensity than the band defined by the matrix. This suggests that nonequilibrium holes from defect states of the matrix are trapped to a larger degree directly at the acceptor level and then recombine with electrons at the size-quantization level.

5. CONCLUSIONS

In the study, the room-temperature absorption, PL and PLE spectra of CdS NCs in the LB matrix are explored before and after the thermal desorption of the matrix at 150 and 200°C. It is shown that the PL band observed in the red region is produced by the recombination of an electron at the size-quantization level and a hole at the acceptor level in the band gap of NCs. It is established that electron excitation is efficiently transferred from the organic matrix to NCs; however, as the desorption temperature is elevated, the efficiency of excitation transfer decreases because of structural disruption of the matrix. A large Stokes shift is observed and interpreted in the context of the model of bright and dark excitons. The Stokes shift increases, as the NC radius is decreased, and corresponds to 220 meV at the NC radius 2.0 nm. In character, the dependence of the Stokes shift on the NC radius is in agreement with theoretical and experimental dependences; however, the shift as such is several times larger than the Stokes shift observed previously. This discrepancy can be attributed to the effect of a matrix with a finite value of the relative permittivity.

ACKNOWLEDGMENTS

We are grateful to L.L. Sveshnikova for placing at our disposal the samples and to A.K. Gutakovskii for recording the TEM images of NCs.

The study was supported by the Russian Foundation for Basic Research, project no. 17-02-01364.

REFERENCES

1. A. Rauadel-Teixier, J. Leluoup, and A. Barraud, Mol. Cryst. Liq. Cryst. **134**, 347 (1986).
2. A. A. Zarubanov and K. S. Zhuravlev, Semiconductors **49**, 380 (2015).
3. D. Baran, A. Balan, S. Celebi, B. M. Esteban, H. Neugebauer, N. S. Sariciftci, and L. Toppare, Chem. Mater. **22**, 2978 (2010).
4. K. M. Coakley and M. D. McGehee, Chem. Mater. **16**, 4533 (2004).
5. M. He, F. Qiu, and Z. Lin, J. Phys. Chem. Lett. **4**, 1788 (2013).
6. L. Wang, Y. Liu, X. Jiang, D. Qin, and Y. Cao, J. Phys. Chem. C **111**, 9538 (2007).
7. D. J. Milliron, A. P. Alivisatos, C. Pitois, C. Edder, and J. Fréchet, Adv. Mater. **15**, 58 (2003).
8. P. Maity, T. Debnath, and H. N. Ghosh, J. Phys. Chem. Lett. **4**, 4020 (2013).
9. N. C. Greenham, X. Peng, and A. P. Alivisatos, Phys. Rev. B **54**, 17628 (1996).
10. Sh. Jin, R. D. Harris, B. Lau, K. O. Aruda, V. A. Amin, and E. A. Weiss, Nano Lett. **14**, 5323 (2014).
11. P. V. Kamat, J. Phys. Chem. Lett. **4**, 908 (2013).
12. T. S. Shamirzaev, D. S. Abramkin, A. V. Nenashev, K. S. Zhuravlev, F. Trojánek, B. Dzurmák, and P. Malý, Nanotechnology **21**, 155703 (2010).
13. F. Gindele, U. Woggon, W. Langbein, J. M. Hvam, K. Leonardi, D. Hommel, and H. Selke, Phys. Rev. B **60**, 8773 (1999).
14. M. Funato, K. Omae, Y. Kawakami, Sg. Fujita, C. Bradford, A. Balocchi, K. A. Prior, and B. C. Cavenett, Phys. Rev. B **73**, 245308 (2006).
15. P. Maity, T. Debnath, and H. N. Ghosh, J. Phys. Chem. Lett. **4**, 4020 (2013).
16. D. S. Ginger and N. C. Greenham, Phys. Rev. B **59**, 10622 (1999).
17. E. A. Bagaev, K. S. Zhuravlev, L. L. Sveshnikova, and D. V. Shcheglov, Semiconductors **42**, 702 (2008).
18. L. E. Brus, J. Chem. Phys. **80**, 4403 (1984).
19. H. Fu and A. Zunger, Phys. Rev. B **56**, 1496 (1997).
20. Zh. Yu, J. Li, D. B. O'Connor, L.-W. Wang, and P. F. Barbara, J. Phys. Chem. B **107**, 5670 (2003).
21. V. A. Fonoberov, E. P. Pokatilov, and A. A. Balandin, Phys. Rev. B **66**, 085310 (2002).
22. K. A. Svit and K. S. Zhuravlev, J. Phys. Chem. C **119**, 19496 (2015).
23. M. Fahlman and W. R. Salaneck, Surf. Sci. **500**, 904 (2002).

Translated by E. Smorgonskaya